ACS OMEGA

http://pubs.acs.org/journal/acsodf

Article

Synthesis, Characterization, and Hydrogen Evolution Activity of Metallo-*meso*-(4-fluoro-2,6-dimethylphenyl)porphyrin Derivatives

Pallas Chou,[†] Lauren Kim,[†] Sammer M. Marzouk,[†] Rui Sun, Alaina C. Hartnett, Dilek K. Dogutan,* Shao-Liang Zheng, and Daniel G. Nocera*

Cite This: *ACS Omega* 2022, 7, 8988–8994

Read Online

ACCESS | Metrics & More | Article Recommendations | Supporting Information

ABSTRACT: Zn(II), Cu(II), and Ni(II) 5,10,15,20-tetrakis(4-fluoro-2,6-dimethylphenyl)porphyrins (TFPs) have been synthesized and characterized. The electronic spectroscopy and cyclic voltammetry of these compounds, along with the free-base macrocycle (2H-TFP), have been determined; 2H-TFP was also structurally characterized by X-ray crystallography. The Cu(II)TFP exhibits catalytic activity for the hydrogen evolution reaction (HER). The analysis of linear sweep voltammograms shows that the HER reaction of Cu(II)TFP with benzoic acid is first-order in proton concentration with an average apparent rate constant for HER catalysis of k_{app} = 5.79 ± 0.47 × 10^3 M^{-1} s^{-1}.

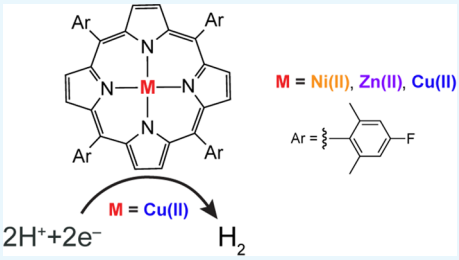

INTRODUCTION

Porphyrin macrocycles have found prominence in applications of catalysis,[1−5] medicine,[6−11] bioimaging,[12,13] molecular electronics,[14−16] information storage,[17,18] and optical imaging[19] as well as energy conversion transformations.[20,21] Metalloporphyrins are especially promising as catalysts for the activation of small molecules of energy consequence including carbon dioxide reduction,[22−26] oxygen reduction reaction,[27−29] and hydrogen evolution reaction (HER).[30−34] Interest in the latter reaction is driven by the potential utility of hydrogen (H_2) as a form of renewable energy storage[35] and consequently plays a key role in sustainable fuel cycles,[36−38] especially as hydrogen fuel cells become increasingly popular.[39−41]

These diverse applications of porphyrin macrocycles, which consist of four pyrrole rings interconnected *via* methene bridges, are derived from functionalization of their peripheries,[42] thus allowing structure−function properties to be tuned with fidelity. In this study, we focus on metalloporphyrins functionalized at the meso position of the macrocyclic ring and substituted with the electron-withdrawing 4-fluoro-2,6-dimethylphenyl group, which was chosen as fluorine provides a convenient handle for porphyrin characterization of new metalated complexes. The free-base 5,10,15,20-tetrakis(4-fluoro-2,6-dimethylphenyl)porphyrin (2H-TFP) platform has been metalated with Fe and shown to support oxidative chemistry; heterolytic cleavage of bound hypochlorite produces the compound I analogue ($TFP^{•+}$)Fe(IV)(O).[43] We now report the reductive chemistry of 2H-TFP with late metals of the first-row transition metal series. The 2H-TFP has been structurally characterized and metalated with Ni(II), Cu(II), and Zn(II). We posited that the late metals such as Cu(II) may exhibit enhanced rates of HER catalytic activity. We show by cyclic voltammetry coupled to chemical analysis that Cu(II)-TFP is an HER catalyst, and the analysis of the electrocatalytic waveform reveals an appreciable rate of HER as compared to previous porphyrin electrocatalysts.[30,44,45]

EXPERIMENTAL SECTION

General Considerations. Free-base *meso*-(4-fluoro-2,6-dimethylphenyl)porphyrin (TFP) was purchased from Frontier Scientific. $Cu(OAc)_2·H_2O$, $Ni(OAc)_2·4H_2O$, and anhydrous $Zn(OAc)_2$ were purchased from Sigma-Aldrich. Hexanes, CH_2Cl_2, MeOH, $CHCl_3$, acetic acid, Na_2SO_4, and NaCl were used as received. Tetrabutylammonium hexafluorophosphate ($TBAPF_6$) was obtained from Sigma-Aldrich, recrystallized from EtOH, dried for two days under vacuum at a Schlenk line without heat, and stored in a nitrogen-filled glovebox. Electrolyte solutions were stored over activated 3 Å molecular sieves before use. ^{1}H NMR spectra were recorded at the Harvard University Department of Chemistry and Chemical Biology NMR facility on a JEOL ECZ400S spectrometer operating at 400 MHz. Absorption spectra were taken with a 1.0 cm quartz cuvette on a Varian Cary 5000 UV−vis-NMR spectrophotometer. Steady-state emission spectra were measured on a fluorimeter (Photon Technology International, PTI model QM4) coupled to a 150 W Xe arc lamp as an excitation light source. Mass spectrometry was performed at the Harvard Center for Mass Spectrometry.

Received: January 6, 2022
Accepted: February 18, 2022
Published: March 2, 2022

https://doi.org/10.1021/acsomega.2c00109
ACS Omega 2022, 7, 8988−8994

Synthesis. *5,10,15,20-Tetrakis(4-fluoro-2,6-dimethylphenyl)porphyrinato-Ni(II).* Free-base 5,10,15,20-tetrakis(4-fluoro-2,6-dimethylphenyl)porphyrin (30 mg, 0.0376 mmol) and $Ni(OAc)_2{\cdot}4H_2O$ (140 mg, 0.564 mmol) were dissolved in acetic acid (15 mL). The resulting solution was heated at reflux for 3 h and then cooled to room temperature. The solvent was removed *in vacuo*, and the residue was subsequently redissolved in CH_2Cl_2 (10 mL), treated with TEA (1 mL), washed with water and brine, and dried over Na_2SO_4. The crude porphyrin solution was concentrated to dryness, and the resulting solid was dissolved in CH_2Cl_2 (10 mL). The crude porphyrin solution was introduced onto a silica column and eluted with a gradient of 0−40% CH_2Cl_2/hexanes. The title compound was isolated as a dark-purple powder (25 mg, 78% isolated yield). ^{1}H NMR (400 MHz, CD_2Cl_2): δ (ppm) 8.54 (s, 8H), 7.13 (d, J = 9.6 Hz, 8H), 1.84 (s, 24H). ^{19}F NMR (400 MHz, CD_2Cl_2): δ (ppm) −116.14 (s). ESI-TOF MS [(M + H)$^+$, M = $C_{52}H_{40}F_4N_4Ni$] (m/z): calcd (obsd), 854.2537 (854.2534).

5,10,15,20-Tetrakis(4-fluoro-2,6-dimethylphenyl)-porphyrinato-Zn(II). Free-base 5,10,15,20-tetrakis(4-fluoro-2,6-dimethylphenyl)porphyrin (30 mg, 0.0376 mmol) was dissolved in $CHCl_3$ (60 mL). In a separate round-bottom flask, anhydrous $Zn(OAc)_2$ (103 mg, 0.564 mmol) was dissolved in MeOH (10 mL). The resulting $Zn(OAc)_2$ solution was added into the porphyrin solution, and the mixture was heated at reflux for 3 h and then cooled to room temperature. The solvent was removed *in vacuo*, and the residue was subsequently redissolved in CH_2Cl_2 (10 mL). The resulting crude porphyrin solution in CH_2Cl_2 was introduced onto a silica column with a syringe and eluted with a gradient of 0−40% hexanes/CH_2Cl_2. The title compound was isolated as a purple powder (28 mg, 86% isolated yield). ^{1}H NMR (400 MHz, $CDCl_3$): δ (ppm) 8.69 (s, 8H), 7.20 (d, J = 9.7 Hz, 8H), 1.84 (s, 24H). ^{19}F NMR (376 MHz, $CDCl_3$): δ (ppm) −116.61 (s). ESI-TOF MS [(M + H)$^+$, M = $C_{52}H_{40}F_4N_4Zn$] (m/z): calcd (obsd), 861.2553 (861.2535).

5,10,15,20-Tetrakis(4-fluoro-2,6-dimethylphenyl)-porphyrinato-Cu(II). Free-base 5,10,15,20-tetrakis(4-fluoro-2,6-dimethylphenyl)porphyrin (30 mg, 0.0376 mmol) and $Cu(OAc)_2{\cdot}H_2O$ (112 mg, 0.564 mmol) were dissolved in acetic acid (15 mL). The solution was heated at reflux for 3 h and cooled to room temperature. The solvent was removed *in vacuo*, and the residue was subsequently redissolved in CH_2Cl_2 (10 mL), treated with TEA (1 mL), washed with water and brine, and dried over Na_2SO_4. The resulting CH_2Cl_2 solution was introduced onto a silica column and eluted with a gradient of 10−60% hexanes/CH_2Cl_2. The title compound was isolated as an orange-red powder (22 mg, 69% isolated yield). ESI-TOF MS [(M + H)$^+$, M = $C_{52}H_{40}CuF_4N_4$] (m/z): calcd (obsd), 860.2558 (860.2534).

Crystallography. Crystals were grown through vapor-diffusion of hexanes into pyridine solution of 2H-TFP at 3 °C. X-ray diffraction data were collected on a Bruker three-circle platform goniometer equipped with an APEX II CCD detector and an Oxford Cryosystems cryostat cooling device using φ and ω scans. A fine-focus sealed tube Cu Kα (1.54178 Å) X-ray source was used. The crystal was mounted on a cryoloop using Paratone oil. The crystal is a four-component non-merohedral twin, and the useful data in the hkl5 format were created by using CELL NOW/Twinabs in the APEX3 program suit. The structure was solved by intrinsic phasing using SHELXT and refined against F^2 on all data by full-matrix least-squares with SHELXL. All non-hydrogen atoms were located in the difference density maps (obtained using Fourier coefficients) and refined anisotropically. Hydrogen atoms were added at calculated positions and refined with a riding model. The disordered solvent could not be located in the Fourier map and was squeezed out by using PLATON/SQUEEZE. Crystal data, data collection, and structure refinement details are included in Table S1.

Electrochemical Methods. All electrochemical experiments were performed with a CH Instruments 760D electrochemical workstation (Austin, Texas) and CHI Version 10.03 software in a N_2-filled glovebox. For cyclic voltammetry and hydrogen electrocatalysis experiments, a three-electrode undivided cell configuration was used with a BASi 3 mm diameter glassy carbon working electrode and a Pt wire auxiliary electrode. The working electrode was polished between each measurement. For bulk electrolysis experiments, a H-cell was used; the working electrode was a glassy carbon plate of 2 cm^2, and the auxiliary electrode was a Pt mesh. The reference electrode for all electrochemical experiments was a BASi Ag wire immersed in the 0.1 M $TBAPF_6$ solution in CH_2Cl_2, and ferrocene was used as an internal standard to define the reference potential. All experiments were performed at room temperature (25 ± 1 °C).

Fluorescence Lifetime Measurements. Time-resolved emission spectra were collected with a Hamamatsu C4334 Streak Scope camera placed perpendicular to the excitation path. The polarizer in the excitation path was set parallel to the excitation pulse, and the polarizer in the emission path was set to the magic angle (54.7°) relative to the parallel one. Measurements were taken in CH_2Cl_2 under nitrogen and in the presence of air. All samples were excited with 400 nm light generated using an OPerA Solo (Coherent) femtosecond optical parametric amplifier seeded with fundamental pulses (800 nm, ∼50 fs) from a Ti:sapphire regenerative amplifier (Coherent Libra-HE). Measurements were made with the following streak camera settings: a slit width of 2000, a grating of 100 g mm^{-1} blazed at 450 nm, and a ruling of 100. Time-resolved emission spectra were the result of the integration of 15,000 exposures. After integration over wavelength, the emission decay curves were fit to a single or biexponential decay function in Logger Pro 3.14.1.

RESULTS AND DISCUSSION

Synthesis of Metalloporphyrins. The synthetic schemes to incorporate the metals of Ni(II), Cu(II), and Zn(II) into 2H-TFP are shown in Figure 1. Metalation reactions were conducted using the metal acetate salts followed by workup and silica gel chromatography to obtain the target porphyrins

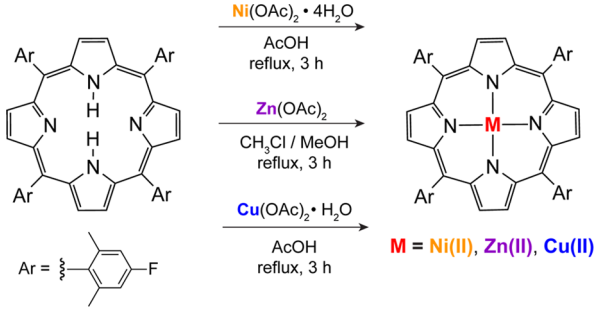

Figure 1. Synthesis schematic of metal porphyrins.

https://doi.org/10.1021/acsomega.2c00109
ACS Omega 2022, 7, 8988−8994

between 69 and 86% isolated yields. ^{1}H NMR spectra for Ni(II)TFP and Zn(II)TFP (Figure S1) were consistent with expectations, where each showed a loss of the pyrrolic N−H resonance in the 2H-TFP upon metalation, as well as the expected chemical shifts and integrations for the porphyrin macrocycle. The corresponding ^{19}F NMR spectra of Ni(II)-TFP and Zn(II)TFP (Figure S2) showed the expected singlet. Given its paramagnetism, NMR spectra were not collected for Cu(II)TFP. The S = 1/2 ground state of Cu(II)TFP is consistent with the effective magnetic moment of 1.55 μ_B as measured by the Evans method.

The TFP macrocycle has been crystallographically characterized, as shown in Figure 2. The porphyrin crystallizes in the

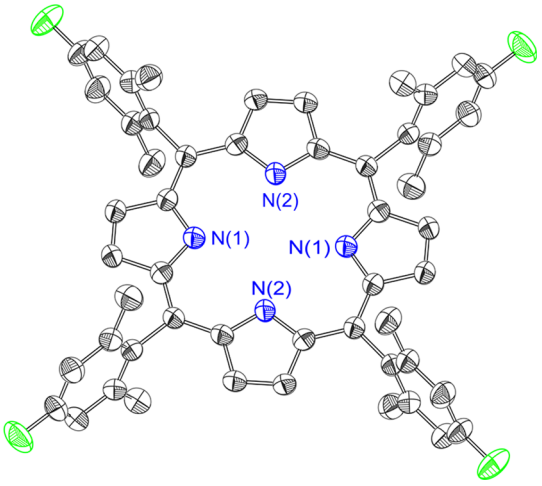

Figure 2. Crystal structure of TFP. Hydrogen atoms have been omitted for clarity.

$P\bar{1}$ space group with half of the macrocycle contained in the asymmetric unit. The inner pyrrolic H-atoms are disordered about the two N-atoms in the asymmetric unit and modeled with an occupancy of 0.5, engendering D_{4h} molecular symmetry. Consistent with this molecular symmetry, the distance between each pair of nitrogen atoms was equal (d[N(1)···N(1)] = 4.11(2) Å and d[N(2)···N(2)] = 4.11(2) Å). The ring is nearly planar with a deviation of 0.03(2) Å for the 4 − N least-squares plane.

Electronic Spectroscopy. The UV−vis spectra for 2H-TFP, Ni(II)TFP, Cu(II)TFP, and Zn(II)TFP, shown in Figure 3, are dominated by the Soret and Q band absorptions of the four-state Gouterman model.[46] As typically observed, the high D_{4h} symmetry of the metalated porphyrins leads to a single Q-band as compared to 2H-TFP. The red-shift of the Soret and Q bands across the period from Ni to Zn TFP is consistent with previous observations of metalloporphyrins.[47]

As expected for metalloporphyrins with partially occupied d-orbitals, the Ni(II) and Cu(II)TFPs exhibit no appreciable emission owing to fast non-radiative decay from the porphyrin π-aromatic chromophore *via* the d-orbital state manifold. In the absence of this non-radiative pathway, the 2H-TFP and the d^{10} Zn(II)TFP porphyrins are highly emissive (Figure 3A,C). Laser excitation of solutions of Zn(II)TFP under N_2 yields emission with a monotonic lifetime decay of 2.27 ns; the emission of 2H-TFP exhibits a biphasic decay of 1.26/8.72 ns under N_2 (Figure S3). Consistent with the assignment of the emission to a fluorescent-excited state, the excited state decay lifetimes are unaffected by the presence of oxygen (τ_o = 2.39 ns for Zn(II)TFP in air and 0.81/9.06 ns for 2H-TFP in air).

Electrochemistry. The cyclic voltammograms (CVs) of the TFP series of porphyrins are shown in Figure 4. The 2H-TFP shows reversible anodic and cathodic waves ($E_{1/2}$ = 0.60 and −1.80 V, respectively) in the potential window scanned, whereas the metalated porphyrins all show two reversible anodic waves and one reversible cathodic wave, except for Ni(II)TFP for which the reduction wave is irreversible. This irreversibility is indicative of a reaction of DCM with the reduced porphyrin. Consistent with this contention, the CV of Ni(II)TFP becomes reversible in non-halogenated solvents.

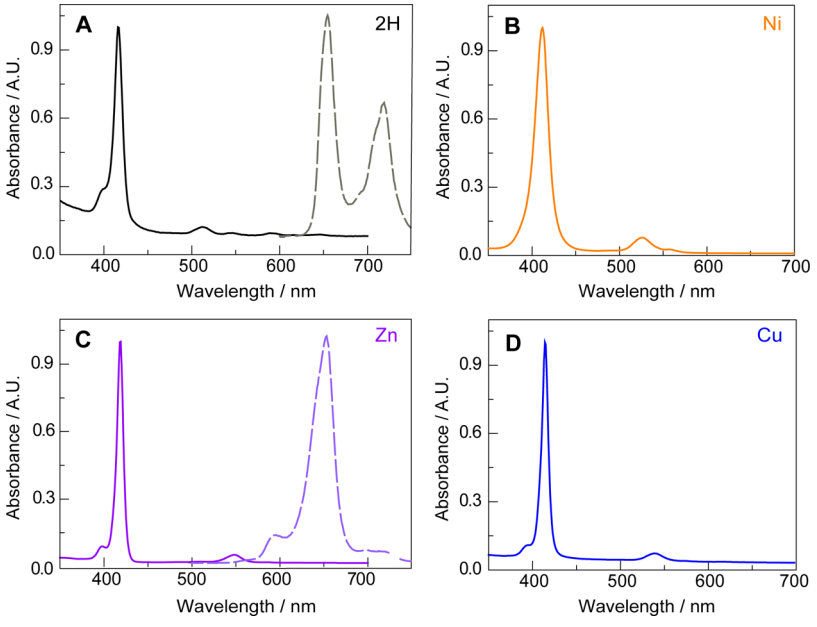

Figure 3. UV−vis absorption spectra of (A) 2H-TFP, (B) Ni(II)TFP, (C) Zn(II)TFP, and (D) Cu(II)TFP. Solutions of 2H-TFP and Zn(II)TFP also exhibited emission, the spectra for which are shown by the dashed line [λ_{exc} = 430 nm for 2H-TFP and 432 nm for Zn(II)TFP]. The absorption and emission spectra are in arbitrary units (A.U.). The spectra were recorded in CH_2Cl_2.

https://doi.org/10.1021/acsomega.2c00109
ACS Omega 2022, 7, 8988−8994

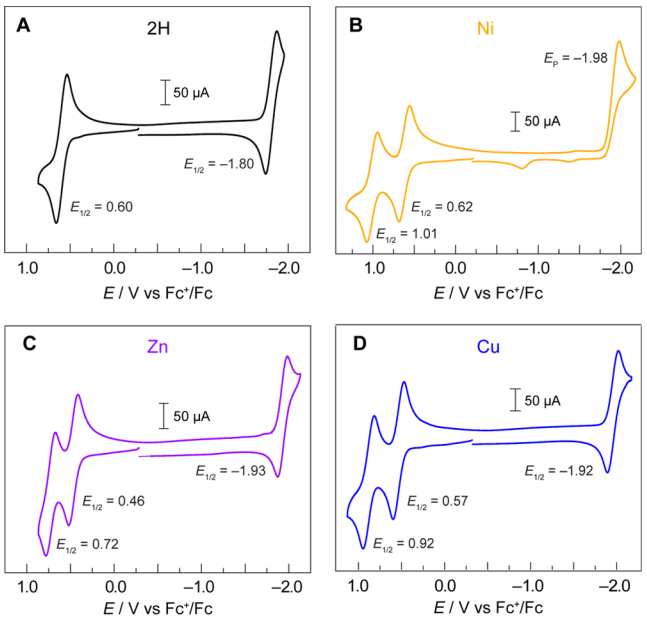

Figure 4. Cyclic voltammograms of (A) 2H-TFP, (B) Ni(II)TFP, (C) Zn(II)TFP, and (D) Cu(II)TFP in CH_2Cl_2 with a 0.1 M $TBAPF_6$-supporting electrolyte. All CVs were recorded in a three-compartment cell with a glassy carbon working electrode, a Pt auxiliary electrode, and a Ag wire dipped in 0.1 M $TBAPF_6$ solution and ferrocene as an internal reference electrode at a scan rate of ν = 100 mV s^{-1}.

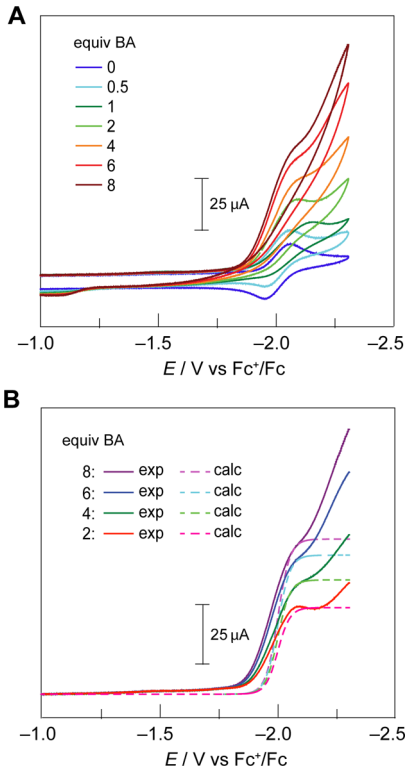

Figure 5. (A) CVs of Cu(II)TFP in CH_2Cl_2 with a 0.1 M $TBAPF_6$-supporting electrolyte with the addition of varying equivalents of BA. Upon the addition of acid, the electrode was polished between scans except for the 1 equiv BA scan. (B) LSV (solid line) and the calculated current trace (dashed line) using eq 1. LSV traces were corrected for the capacitive current at −1.0 V *vs* Fc^+/Fc. All CVs were recorded with a glassy carbon button (3 mm diameter) working electrode, a Pt auxiliary electrode, and a Ag wire reference electrode at a scan rate of ν = 100 mV s^{-1}.

For instance, although only slightly soluble in acetonitrile, a reversible reduction wave is observed (Figure S4). The electrochemistry shown in Figure 4 is typical of metalloporphyrins, with the oxidations assigned to the generation of the π-cation radical and dication, and the reduction to the π-radical anion of the porphyrin ring.[48] As originally reported by Wolberg and Manassen, the Cu and Zn porphyrins within a homologous series are more easily oxidized than the Ni (as well as Fe and Co) analogue.[49] Moreover, the redox chemistry follows the trend originally identified by Furhop, Kadish, and Davis that the ΔE between the radical anion and cation is more or less constant (ΔE = 2.44 ± 0.05), indicative of a similar HOMO−LUMO gap across a homologous series.[50] However, for the reversible couples, there is an inverse relation for the ease of metalloporphyrin ring oxidation and the ease of metalloporphyrin ring reduction, which has been attributed[50] to be a result of electrostatic and electronegativity effects of the divalent metal ion residing within the macrocycle cavity.

HER Catalysis. The CV of Cu(II)TFP in the presence of an acid is indicative of HER catalysis. CVs of 0.6 mM Cu(II)TFP were recorded in the presence of 0−8 equiv of benzoic acid (BA) (Figure 5A). BA is a good proton source as its comparative mild acidity (pK_a = 20.7 in acetonitrile[51]) does not induce demetalation of Cu(II)TFP. In agreement with catalytic HER behavior, the cathodic wave increases in current with the addition of BA, with a concomitant loss of reversibility (Figure 5A). The irreversibility of the reduction wave with acid addition is consistent with an ECEC mechanism where the reduced porphyrin is protonated, followed by further reduction and protonation to produce H_2.[52−55] The analysis of the gaseous headspace by gas chromatography of bulk-electrolyzed solutions of 1.12 mM Cu(II)TFP in the presence of 15.4 mM BA confirms the production of H_2, which is linearly produced and will consume current (Figure S5). At the completion of bulk electrolysis, the solution was analyzed by TLC and there was no evidence of demetalated porphyrin. Additionally, the UV−visible absorption spectra of electrolyzed solutions match those of the original solution. At low BA concentrations, the peak-shaped CV is characteristic of mass-transported limitations on the substrate. However, as the proton concentration is increased, the peak-shaped CV is less pronounced and approaches the canonical S-shape where catalysis is governed by pure kinetic control of the reaction without the consumption of substrate becoming limiting.[56] The S-shape is evident from the linear scan voltammograms (LSVs) shown in Figure 5B, although we note that at large negative potentials, the plateau region is convoluted with background H_2 generation from the glassy carbon electrode.

The catalytic HER activity may be quantified by normalizing the observed current under catalytic conditions, i, to the current of the one-electron wave associated with the reduction of Cu(II)TFP, i_p^0. In this way, the magnitude of i/i_p^0 establishes whether the experimental current response is catalytic; in the case of HER, the catalytic regime for the two-electron reduction of $2H^+$ to H_2 is attained when $i/i_p^0 > 2$. The i/i_p^0 ratio of >2 for BA concentrations >2 equiv is indicative of HER catalytic activity.

From the quasi-plateau current, the HER efficacy of Cu(II)TFP may be ascertained by fitting the canonical S-shaped catalytic CVs to[52,57]

https://doi.org/10.1021/acsomega.2c00109
ACS Omega 2022, 7, 8988−8994

$$i = \frac{i_{pl}}{1 + \exp\left[\frac{F}{RT}(E - E_{1/2})\right]} \quad (1)$$

where i is the theoretical current response, i_{pl} is the experimentally derived plateau current, F is Faraday's constant, R is the gas constant, T is the temperature, E is the applied potential, and $E_{1/2}$ is the experimentally derived half-wave potential. Figure 5B shows the fits to eq 1 for Cu(II)TFP. We note that the inflection point of the plateau current prior to the increase in background current at large negative potentials is modeled well by eq 1.

The maximum turnover frequencies, TOF_{max}, at each concentration of BA are provided from[57]

$$TOF_{max} = \left[\frac{i_{pl}}{FSC^{0}_{Cu}\sqrt{2 \cdot D_{Cu}}}\right]^2 \quad (2)$$

where S is the surface area of the electrode, $C_{Cu}{}^{0}$ is the concentration of the Cu(II)TFP catalyst, and D_{Cu} is the diffusion constant of the Cu(II)TFP catalyst based on that measured for typical porphyrins ($D = 5 \times 10^{-6}$ cm^2 s^{-1}[58]). The catalytic rate constant, which is the determinant of the plateau current, is related to the TOF_{max} by

$$TOF_{max} = k_{app} \cdot C_{BA} \quad (3)$$

Table S2 lists the k_{app} obtained from eqs 2 and 3 for each concentration of BA, yielding an average apparent rate constant for HER catalysis of $k_{app} = 5.79 \pm 0.47 \times 10^3$ M^{-1} s^{-1}. Additionally, the log(TOF_{max}) values for Cu(II)TFP at every log[BA] concentration are shown in Figure S6. The slope of the line furnishes a reaction order of unity with respect to the acid across the range of [BA], indicating that the HER rate is first order in proton concentration, consistent with the rate-determining step involving protonation of the reduced porphyrin in the ECEC process. We note that the half-wave potential (potential when the current is half of the plateau current) is slightly shifted from the standard potential of the catalyst, as observed from the anodic shifts of the experimental LSV from the calculated LSV in Figure 5B. This shift may be indicative that the rate-determining step is not the first irreversible protonation step after reduction but is rather the second chemical step to produce H_2.

CONCLUSIONS

We report the synthesis and characterization of Ni(II)TFP, Cu(II)TFP, and Zn(II)TFP and the structural characterization of the free-base parent porphyrin 2H-TFP. The M(II)TFP series possesses prototypical spectral and redox properties of metalloporphyrins. In the case of Cu(II)TFP, its CVs indicate HER catalytic activity. Hydrogen generation is consistent with an ECEC mechanism that is first order in proton concentration with an apparent HER rate constant for catalysis of $5.79 \pm 0.47 \times 10^3$ M^{-1} s^{-1}, as determined from the analysis of the catalytic traces of LSVs. These studies expand upon the growing body of literature on using metalloporphyrins as catalysts for energy conversion transformations.

ASSOCIATED CONTENT

Supporting Information

The Supporting Information is available free of charge at https://pubs.acs.org/doi/10.1021/acsomega.2c00109.

^{1}H and ^{19}F NMR spectra, crystal structure and refinement table, Ni(II)TFP CV, excited state decay curves and fits, data obtained from fits of eqs 2 and 3 to LSV traces, and plot to determine the proton reaction order (PDF)

Crystallographic data for 2H-TFP(CIF)

Accession Codes

Metrical data for the solid-state structures are available from the Cambridge Crystallographic Data Centre under the reference number CCDC 2127619, which contains the supplementary crystallographic data for this paper. These data can be obtained free of charge *via* www.ccdc.cam.ac.uk/data_request/cif, by emailing at data_request@ccdc.cam.ac.uk, or by contacting The Cambridge Crystallographic Data Centre, 12 Union Road, Cambridge CB2 1EZ, UK; fax: +44 1223 336033.

AUTHOR INFORMATION

Corresponding Authors

Dilek K. Dogutan − *Department of Chemistry and Chemical Biology, Harvard University, Cambridge, Massachusetts 02138, United States;* orcid.org/0000-0002-2935-4393; Email: dkiper@fas.harvard.edu

Daniel G. Nocera − *Department of Chemistry and Chemical Biology, Harvard University, Cambridge, Massachusetts 02138, United States;* orcid.org/0000-0001-5055-320X; Email: dnocera@fas.harvard.edu

Authors

Pallas Chou − *Department of Chemistry and Chemical Biology, Harvard University, Cambridge, Massachusetts 02138, United States*

Lauren Kim − *Department of Chemistry and Chemical Biology, Harvard University, Cambridge, Massachusetts 02138, United States*

Sammer M. Marzouk − *Department of Chemistry and Chemical Biology, Harvard University, Cambridge, Massachusetts 02138, United States;* orcid.org/0000-0002-4250-582X

Rui Sun − *Department of Chemistry and Chemical Biology, Harvard University, Cambridge, Massachusetts 02138, United States;* orcid.org/0000-0002-3894-8425

Alaina C. Hartnett − *Department of Chemistry and Chemical Biology, Harvard University, Cambridge, Massachusetts 02138, United States*

Shao-Liang Zheng − *Department of Chemistry and Chemical Biology, Harvard University, Cambridge, Massachusetts 02138, United States;* orcid.org/0000-0002-6432-9943

Complete contact information is available at: https://pubs.acs.org/10.1021/acsomega.2c00109

Author Contributions

†P.C., L.K., and S.M.M. contributed equally.

Funding

This work was supported by the Solar Photochemistry Program of the Chemical Sciences, the Geosciences and Biosciences Division, and the Office of Basic Energy Sciences of the U.S. Department of Energy DE-SC0017619.

Notes

The authors declare no competing financial interest.

■ ACKNOWLEDGMENTS

We thank Cyrille Costentin for valuable discussions pertaining to simulations of CVs, Shelby E. Elder for assistance in making lifetime measurements, and Miguel Gonzalez for GC hydrogen measurements.

■ REFERENCES

(1) Costa e Silva, R.; Oliveira da Silva, L.; de Andrade Bartolomeu, A.; Brocksom, T. J.; de Oliveira, K. T. Recent Applications of Porphyrins as Photocatalysts in Organic Synthesis: Batch and Continuous Flow Approaches. *Beilstein J. Org. Chem.* **2020**, *16*, 917−955.

(2) Barona-Castaño, J.; Carmona-Vargas, C.; Brocksom, T.; de Oliveira, K. Porphyrins as Catalysts in Scalable Organic Reactions. *Molecules* **2016**, *21*, 310.

(3) Aguirre-Araque, J. S.; Toma, H. E. Catalytic Properties of Supramolecular Polymetallated Porphyrins. *Phys. Sci. Rev.* **2021**, DOI: 10.1515/psr-2019-0054, [Online].

(4) Feng, L.; Wang, K.-Y.; Joseph, E.; Zhou, H.-C. Catalytic Porphyrin Framework Compounds. *Trends Chem.* **2020**, *2*, 555−568.

(5) Rybicka-Jasińska, K.; Shan, W.; Zawada, K.; Kadish, K. M.; Gryko, D. Porphyrins as Photoredox Catalysts: Experimental and Theoretical Studies. *J. Am. Chem. Soc.* **2016**, *138*, 15451−15458.

(6) Kurniawan, F.; Miura, Y.; Kartasasmita, R.; Yoshioka, N.; Mutalib, A.; Tjahjono, D. In Silico Study, Synthesis, and Cytotoxic Activities of Porphyrin Derivatives. *Pharmaceuticals* **2018**, *11*, 8.

(7) Pucelik, B.; Paczyński, R.; Dubin, G.; Pereira, M. M.; Arnaut, L. G.; Dąbrowski, J. M. Properties of Halogenated and Sulfonated Porphyrins Relevant for the Selection of Photosensitizers in Anticancer and Antimicrobial Therapies. *PLoS One* **2017**, *12*, No. e0185984.

(8) Lin, Y.; Zhou, T.; Bai, R.; Xie, Y. Chemical Approaches for the Enhancement of Porphyrin Skeleton-Based Photodynamic Therapy. *J. Enzyme Inhib. Med. Chem.* **2020**, *35*, 1080−1099.

(9) Dolmans, D. E. J. G. J.; Fukumura, D.; Jain, R. K. Photodynamic Therapy for Cancer. *Nat. Rev. Cancer* **2003**, *3*, 380−387.

(10) Boyle, R. W.; Dolphin, D. Structure and Biodistribution Relationships of Photodynamic Sensitizers. *Photochem. Photobiol.* **1996**, *64*, 469−485.

(11) Mroz, P.; Pawlak, A.; Satti, M.; Lee, H.; Wharton, T.; Gali, H.; Sarna, T.; Hamblin, M. R. Functionalized Fullerenes Mediate Photodynamic Killing of Cancer Cells: Type I versus Type II Photochemical Mechanism. *Free Radical Biol. Med.* **2007**, *43*, 711−719.

(12) Imran, M.; Ramzan, M.; Qureshi, A.; Khan, M.; Tariq, M. Emerging Applications of Porphyrins and Metalloporphyrins in Biomedicine and Diagnostic Magnetic Resonance Imaging. *Biosensors* **2018**, *8*, 95.

(13) Ptaszek, M. Porphyrins and Hydroporphyrins for *in vivo* Bioimaging. In *Applications of Porphyrinoids as Functional Materials*; Lang, H., Rueffer, T., Ed.; RSC Publishing: London, 2021; Chapter 10.

(14) Aydin, M.; Akins, D. L. Geometric and Electronic Properties of Porphyrin and Its Derivatives. In *Applications of Molecular Spectroscopy to Current Research in the Chemical and Biological Sciences*; Stauffer, M. T., Ed.; InTech, 2016.

(15) Longevial, J. F.; Clément, S.; Wytko, J. A.; Ruppert, R.; Weiss, J.; Richeter, S. Peripherally Metalated Porphyrins with Applications in Catalysis, Molecular Electronics and Biomedicine. *Chem.—Eur. J.* **2018**, *24*, 15442−15460.

(16) Jurow, M.; Schuckman, A. E.; Batteas, J. D.; Drain, C. M. Porphyrins as Molecular Electronic Components of Functional Devices. *Coord. Chem. Rev.* **2010**, *254*, 2297−2310.

(17) Carcel, C. M.; Laha, J. K.; Loewe, R. S.; Thamyongkit, P.; Schweikart, K.-H.; Misra, V.; Bocian, D. F.; Lindsey, J. S. Porphyrin Architectures Tailored for Studies of Molecular Information Storage. *J. Org. Chem.* **2004**, *69*, 6739−6750.

(18) Li, C.; Ly, J.; Lei, B.; Fan, W.; Zhang, D.; Han, J.; Meyyappan, M.; Thompson, M.; Zhou, C. Data Storage Studies on Nanowire Transistors with Self-Assembled Porphyrin Molecules. *J. Phys. Chem. B* **2004**, *108*, 9646−9649.

(19) Licha, K. Contrast Agents for Optical Imaging. In *Contrast Agents II*; Krause, W., de Meijere, A., Kessler, H., Ley, S. V., Thiem, J., Vögtle, F., Houk, K. N., Lehn, J.-M., Schreiber, S. L., Trost, B. M., Yamamoto, H., Series, Eds.; Topics in Current Chemistry; Springer Berlin Heidelberg: Berlin, Heidelberg, 2002; Vol. *222*, pp 1−29.

(20) Gust, D.; Moore, T. A.; Moore, A. L. Solar Fuels via Artificial Photosynthesis. *Acc. Chem. Res.* **2009**, *42*, 1890−1898.

(21) Walter, M. G.; Rudine, A. B.; Wamser, C. C. Porphyrins and Phthalocyanines in Solar Photovoltaic Cells. *J. Porphyr. Phthalocyanines* **2010**, *14*, 759−792.

(22) Costentin, C.; Drouet, S.; Robert, M.; Savéant, J.-M. A Local Proton Source Enhances CO_2 Electroreduction to CO by a Molecular Fe Catalyst. *Science* **2012**, *338*, 90−94.

(23) Costentin, C.; Robert, M.; Savéant, J.-M. Current Issues in Molecular Catalysis Illustrated by Iron Porphyrins as Catalysts of the CO_2-to-CO Electrochemical Conversion. *Acc. Chem. Res.* **2015**, *48*, 2996−3006.

(24) Margarit, C. G.; Asimow, N. G.; Costentin, C.; Nocera, D. G. Tertiary Amine-Assisted Electroreduction of Carbon Dioxide to Formate Catalyzed by Iron Tetraphenylporphyrin. *ACS Energy Lett.* **2020**, *5*, 72−78.

(25) Margarit, C. G.; Schnedermann, C.; Asimow, N. G.; Nocera, D. G. Carbon Dioxide Reduction by Iron Hangman Porphyrins. *Organometallics* **2019**, *38*, 1219−1223.

(26) Costentin, C.; Robert, M.; Savéant, J.-M. Catalysis of the Electrochemical Reduction of Carbon Dioxide. *Chem. Soc. Rev.* **2013**, *42*, 2423−2436.

(27) Pegis, M. L.; Wise, C. F.; Martin, D. J.; Mayer, J. M. Oxygen Reduction by Homogeneous Molecular Catalysts and Electrocatalysts. *Chem. Rev.* **2018**, *118*, 2340−2391.

(28) Martin, D. J.; Wise, C. F.; Pegis, M. L.; Mayer, J. M. Developing Scaling Relationships for Molecular Electrocatalysis through Studies of Fe-Porphyrin-Catalyzed O_2 Reduction. *Acc. Chem. Res.* **2020**, *53*, 1056−1065.

(29) Passard, G.; Dogutan, D. K.; Qiu, M.; Costentin, C.; Nocera, D. G. Oxygen Reduction Reaction Promoted by Manganese Porphyrins. *ACS Catal.* **2018**, *8*, 8671−8679.

(30) Beyene, B. B.; Hung, C.-H. Recent Progress on Metalloporphyrin-Based Hydrogen Evolution Catalysis. *Coord. Chem. Rev.* **2020**, *410*, 213234.

(31) Lei, H.; Wang, Y.; Zhang, Q.; Cao, R. First-Row Transition Metal Porphyrins for Electrocatalytic Hydrogen Evolution—A SPP/JPP Young Investigator Award Paper. *J. Porphyr. Phthalocyanines* **2020**, *24*, 1361−1371.

(32) Sarkar, B.; Chandra, S.; Singha Hazari, A.; Song, Q.; Hunger, D.; Neuman, N. I.; van Slageren, J.; Klemm, E. Remarkable Enhancement of Catalytic Activity of Cu-Complexes in the Electrochemical Hydrogen Evolution Reaction (HER) by Using Triply-Fused Porphyrin. *Chemistry* **2021**, DOI: 10.33774/chemrxiv-2021-f6l32.

(33) Khusnutdinova, D.; Wadsworth, B. L.; Flores, M.; Beiler, A. M.; Reyes Cruz, E. A.; Zenkov, Y.; Moore, G. F. Electrocatalytic Properties of Binuclear Cu(II) Fused Porphyrins for Hydrogen Evolution. *ACS Catal.* **2018**, *8*, 9888−9898.

(34) Margarit, C. G.; Asimow, N. G.; Thorarinsdottir, A. E.; Costentin, C.; Nocera, D. G. Impactful Role of Cocatalysts on Molecular Electrocatalytic Hydrogen Production. *ACS Catal.* **2021**, *11*, 4561−4567.

(35) Lewis, N. S.; Nocera, D. G. Powering the Planet: Chemical Challenges in Solar Energy Utilization. *Proc. Natl. Acad. Sci. U.S.A.* **2006**, *103*, 15729−15735.

(36) Nocera, D. G. The Artificial Leaf. *Acc. Chem. Res.* **2012**, *45*, 767−776.

https://doi.org/10.1021/acsomega.2c00109
ACS Omega 2022, 7, 8988−8994

(37) Dogutan, D. K.; Nocera, D. G. Artificial Photosynthesis at Efficiencies Greatly Exceeding That of Natural Photosynthesis. *Acc. Chem. Res.* **2019**, *52*, 3143−3148.
(38) Di Carlo, G.; Orbelli Biroli, A.; Pizzotti, M.; Tessore, F. Efficient Sunlight Harvesting by A4 β-Pyrrolic Substituted Zn(II) Porphyrins: A Mini-Review. *Front. Chem.* **2019**, *7*, 177.
(39) Staffell, I.; Scamman, D.; Velazquez Abad, A.; Balcombe, P.; Dodds, P. E.; Ekins, P.; Shah, N.; Ward, K. R. The Role of Hydrogen and Fuel Cells in the Global Energy System. *Energy Environ. Sci.* **2019**, *12*, 463−491.
(40) Brandon, N. P.; Kurban, Z. Clean Energy and the Hydrogen Economy. *Philos. Trans. R. Soc., A* **2017**, *375*, 20160400.
(41) Felseghi, R.-A.; Carcadea, E.; Raboaca, M. S.; Trufin, C. N.; Filote, C. Hydrogen Fuel Cell Technology for the Sustainable Future of Stationary Applications. *Energies* **2019**, *12*, 4593.
(42) Hiroto, S.; Miyake, Y.; Shinokubo, H. Synthesis and Functionalization of Porphyrins through Organometallic Methodologies. *Chem. Rev.* **2017**, *117*, 2910−3043.
(43) Yokota, S.; Fujii, H. Critical Factors in Determining the Heterolytic versus Homolytic Bond Cleavage of Terminal Oxidants by Iron(III) Porphyrin Complexes. *J. Am. Chem. Soc.* **2018**, *140*, 5127−5137.
(44) Amanullah, S.; Dey, A. The Role of Porphyrin Peripheral Substituents in Determining the Reactivities of Ferrous Nitrosyl Species. *Chem. Sci.* **2020**, *11*, 5909−5921.
(45) Castro-Cruz, H. M.; Arias-Aranda, L. R.; Farfán, N.; Xochitiotzi-Flores, E.; Macías-Ruvalcaba, N. A. Elucidating the Electroreduction Mechanism of the Monoprotonated Octaethylporphyrin. A Comparative Study with the Diprotonated Octaethyl- and *Meso* -Tetraphenyl-Porphyrins. *J. Electrochem. Soc.* **2020**, *167*, 155507.
(46) Gouterman, M.; Wagnière, G. H.; Snyder, L. C. Spectra of Porphyrins. Part II. Four Orbital Model. *J. Mol. Spectrosc.* **1963**, *11*, 108−127.
(47) Marsh, D.; Mink, L. Microscale Synthesis and Electronic Absorption Spectroscopy of Tetraphenylporphyrin H_2(TPP) and Metalloporphyrins Zn^{II}(TPP) and Ni^{II}(TPP). *J. Chem. Educ.* **1996**, *73*, 1188−1190.
(48) Kadish, K. M. The Electrochemistry of Metalloporphyrins in Nonaqueous Media. *Prog. Inorg. Chem.* **1986**, *34*, 435−605.
(49) Wolberg, A.; Manassen, J. Electrochemical and Electron Paramagnetic Resonance Studies of Metalloporphyrins and Their Electrochemical Oxidation Products. *J. Am. Chem. Soc.* **1970**, *92*, 2982−2991.
(50) Furhop, J. H.; Kadish, K. M.; Davis, D. G. The Redox Behavior of Metallo Octaethylporphyrins. *J. Am. Chem. Soc.* **1973**, *95*, 5140−5147.
(51) Fourmond, V.; Jacques, P.-A.; Fontecave, M.; Artero, V. H_2 Evolution and Molecular Electrocatalysts: Determination of Overpotentials and Effect of Homoconjugation. *Inorg. Chem.* **2010**, *49*, 10338−10347.
(52) Savéant, J. M. *Elements of Molecular and Biomolecular Electrochemistry: An Electrochemical Approach to Electron Transfer Chemistry*; Wiley: Hoboken, NJ, 2006.
(53) Roubelakis, M. M.; Bediako, D. K.; Dogutan, D. K.; Nocera, D. G. Proton-Coupled Electron Transfer Kinetics for the Hydrogen Evolution Reaction of Hangman Porphyrins. *Energy Environ. Sci.* **2012**, *5*, 7737−7740.
(54) Bediako, D. K.; Solis, B. H.; Dogutan, D. K.; Roubelakis, M. M.; Maher, A. G.; Lee, C. H.; Chambers, M. B.; Hammes-Schiffer, S.; Nocera, D. G. Role of Pendant Proton Relays and Proton-Coupled Electron Transfer on the Hydrogen Evolution Reaction by Nickel Hangman Porphyrins. *Proc. Natl. Acad. Sci. U.S.A.* **2014**, *111*, 15001−15006.
(55) Roubelakis, M. M.; Bediako, D. K.; Dogutan, D. K.; Nocera, D. G. Influence of the Proton Relay Spacer on Hydrogen Electrocatalysis by Cobalt Hangman Porphyrins. *J. Porphyr. Phthalocyanines* **2021**, *25*, 714−723.
(56) Savéant, J. M.; Costentin, C. *Elements of Molecular and Biomolecular Electrochemistry*, 2nd ed.; Wiley: Hoboken, NJ, 2019; Chapter 4.
(57) Azcarate, I.; Costentin, C.; Robert, M.; Savéant, J.-M. Dissection of Electronic Substituent Effects in Multielectron-Multistep Molecular Catalysis. Electrochemical CO_2-to-CO Conversion Catalyzed by Iron Porphyrins. *J. Phys. Chem. C* **2016**, *120*, 28951.
(58) Lexa, D.; Rentien, P.; Savéant, J. M.; Xu, F. Methods for Investigating the Mechanistic and Kinetic Role of Ligand Exchange Reactions in Coordination Electrochemistry: Cyclic Voltammetry of Chloroiron(III)tetraphenylporphyrin in Dimethylformamide. *J. Electroanal. Chem. Interfacial Electrochem.* **1985**, *191*, 253−279.

https://doi.org/10.1021/acsomega.2c00109
ACS Omega 2022, 7, 8988−8994